

# **Evolutionary Mechanisms and Reversal Strategies of Acquired Resistance to RC48 in Bladder Cancer**

Chengming Yang, Lushan Yang, Bufan Ying, Shu Bai, Dan Xie, Yuchen Feng, Xingyi Song, Jiaoxue Guo, Xinyue Yu, Huiyun Deng, Xinrui Shang, Siyi Gao, Cheng Zhong, Zihan Zhao, Lianghua Wang, Jianhua Luo, Meng Guo, Yu Kong, Sheng Zhang, Mingjuan Sun\*

\*Correspondence to: Mingjuan Sun (sunmj@smmu.edu.cn)

## **Abstract**

**Objective:** To elucidate the mechanisms of resistance to Disitamab Vedotin (RC48) in human bladder transitional cell carcinoma (BLCA). **Methods:** An RC48-resistant cell line (T24-RC48) was established by stepwise dose-escalation from the parental T24 cells. Phenotypic characterisation comprised CCK-8, proliferation kinetics, Transwell migration/invasion assays, and flow cytometry for cell cycle/apoptosis analysis. Mechanisms were explored using transcriptomic and proteomic sequencing. Key findings were validated via qRT-PCR and Western Blot (WB). Angiogenesis assays were performed to investigate the pro-angiogenic ability of T24-RC48. **Results:** T24-RC48 showed a 10-fold increase in IC<sub>50</sub> relative to parental cells, concomitant with enhanced migration, invasion, reduced G2 arrest, and increased resistance to apoptosis. Integrated omics, qRT-PCR and WB identified upregulation of VEGF, PD-L1, RBPJ, and Notch pathway activation. Ivonescimab inhibits the pro-angiogenic activity potentiated by T24-RC48. **Conclusion:** RC48 resistance involves oxidative stress, angiogenesis, and immune escape. Combining RC48 with ivonescimab may improve outcomes and sustain precision therapy in BLCA.

**Keywords:** Bladder cancer; ADC drug; Drug resistance mechanism; Disitamab Vedotin; Multi-omics analysis

## Introduction

Bladder cancer, particularly bladder urothelial carcinoma (BLCA), represents one of the most common malignancies of the urinary system. With over 610,000 new cases globally in 2022, it was the ninth most common cancer worldwide and caused approximately 220,000 deaths<sup>1</sup>. Prognosis for patients with metastatic disease remains dismal, with a five-year survival rate of only 5% and a median overall survival of 9–15 months. In China, BLCA accounted for 15% of global new cases and 19% of deaths in 2022, highlighting its substantial public health burden. The burden of disease is expected to continue to increase in 2040<sup>2</sup>. Current standard treatments include surgery, chemotherapy, and immunotherapy, yet high recurrence and metastasis rates persist, underscoring the urgent need for more effective therapeutic strategies.

Antibody-drug conjugates (ADCs) have emerged as a promising class of targeted anticancer agents<sup>3</sup>. By combining the specificity of monoclonal antibodies with the potent cytotoxicity of payload drugs, ADCs enable precise delivery of chemotherapeutic agents to tumor cells, thereby minimizing systemic toxicity<sup>4</sup>. ADCs typically undergo antigen binding, internalization, lysosomal degradation, and payload release, leading to tumor cell death via mechanisms such as direct cytotoxicity, inhibition of downstream signaling, antibody-dependent cellular cytotoxicity (ADCC), and bystander effects<sup>5</sup>.

Disitamab Vedotin (RC48) is the first China-originated ADC to receive dual breakthrough therapy designation from both the U.S. FDA and China's NMPA. It targets HER2-expressing tumors and is approved for the treatment of locally advanced or metastatic urothelial carcinoma in patients who have previously received platinum-based chemotherapy<sup>6</sup>. RC48 consists of a novel anti-HER2 monoclonal antibody (disitamab), a cleavable linker, and the cytotoxic payload monomethyl auristatin E (MMAE). Upon binding to HER2, the ADC is internalized, and MMAE is released to inhibit microtubule assembly, inducing apoptosis<sup>7</sup>. Notably, MMAE's membrane permeability enables a potent bystander effect, enhancing antitumor activity against heterogeneous tumors.

Despite these advances, drug resistance remains a major obstacle in ADC therapy. Both intrinsic and acquired resistance limit the clinical efficacy of ADCs across various cancers. Proposed mechanisms of ADC resistance include reduced antigen expression, impaired internalization and trafficking, altered lysosomal function, enhanced drug efflux, and adaptive changes in downstream signaling pathways. For HER2-targeting ADCs like RC48, loss or mutation of HER2 may contribute to resistance<sup>8</sup>. However, the molecular mechanisms underlying RC48 resistance in BLCA are not yet fully understood.

Elucidating these mechanisms is critical for developing strategies to overcome resistance, identifying predictive biomarkers, and guiding combination therapies. In this study, we established an RC48-resistant BLCA cell line (T24-RC48) through stepwise exposure to increasing drug concentrations. We performed comprehensive multi-omics analyses—including transcriptomics and proteomics sequencing—to identify key genetic and proteomic alterations associated with resistance. Functional validation was conducted using qRT-PCR, Western blot, and phenotypic assays. Furthermore, we explored the roles of PD-L1 and VEGF in mediating immune evasion and angiogenesis, respectively. Our findings aim to provide new insights into the resistance mechanisms of RC48 in BLCA and support the development of more effective therapeutic regimens, such as combination therapy with bispecific antibodies targeting both PD-1 and VEGF.

## Results

### T24-RC48 exhibits morphological changes and reduced drug sensitivity

Morphological observation revealed that the RC48-resistant human bladder cancer cell line T24-RC48 exhibited a smaller cell size and a tendency to grow in clusters compared to the parental T24 cells ([Fig. 1a-d](#)). The resistance index, calculated as the ratio of IC<sub>50</sub> values (resistant IC<sub>50</sub> / parental IC<sub>50</sub>), was 10 ([Fig. 1m](#)), indicating significantly reduced sensitivity to RC48 in the resistant cells.

### T24-RC48 maintains proliferation capacity under RC48 treatment

Inverted phase-contrast microscopy showed that after 5 days of culture, all cell lines (T24 wild-type and low/middle/high resistance T24-RC48) maintained good growth status, with intact morphology, tight adhesion, clear edges, and no significant apoptotic bodies or debris. Cell density reached approximately 100% ([Fig. 1e-h](#)). However, after 5 days of treatment with 200 µg/ml RC48, the density of T24 wild-type and low/middle/high resistance T24-RC48 cells decreased significantly. T24 wild-type cells showed extensive detachment and shrinkage, exhibiting typical apoptotic morphology ([Fig. 1i](#)). The low-resistance T24-RC48 cells adhered sparsely, with abnormal morphology making viability difficult to assess ([Fig. 1j](#)). The middle-resistance group retained about 50% cell density, with improved but still abnormal morphology ([Fig. 1k](#)). The high-resistance group showed the highest cell density among all treated groups, with normal morphology and visible mitotic figures, indicating active proliferation ([Fig. 1l](#)).

Without RC48 treatment, all four cell lines exhibited stable proliferation with similar doubling

times ([Fig. 1n](#)). After treatment with 200 µg/ml RC48, the OD value of wild type T24 dropped sharply from 2.1 to 0.48 (77.1% inhibition). The inhibition rates decreased with increasing resistance: low resistance (OD = 0.55, 72.5% inhibition), middle resistance (OD = 0.61, 60.5% inhibition), and high resistance (OD = 1.53, 19.4% inhibition) ([Fig. 1o](#)), confirming a negative correlation between resistance level and drug sensitivity.

### **T24-RC48 shows altered cell cycle distribution upon RC48 exposure**

After 36 hours of RC48 treatment, flow cytometry revealed significant changes in cell cycle distribution. The G2 peak increased markedly in all treated cells, most notably in wild type T24. No visible differences were observed among RC48-resistant cell lines in untreated or treated conditions. However, resistant cells showed distinct G1 and G2 peak positions compared to wild-type cells ([Fig. 2a](#)).

G1 phase proportion decreased significantly ( $P < 0.0001$ ), while G2 phase proportion increased significantly ( $P < 0.0001$ ) in all cells after treatment. Among them, the overall growth rate of G2 phase in the drug-resistant group was lower than that in the wild type. S phase proportion decreased significantly in wild type cells ( $P < 0.05$ ), showed no change in low resistance cells, and increased significantly in middle and high resistance cells ( $P < 0.0001$ ) ([Fig. 2b](#)).

### **Apoptosis resistance is enhanced in T24-RC48**

Apoptosis rates increased in all cell lines after 48 hours of RC48 treatment ([Fig. 2c-d](#)). In the untreated group, the apoptosis rate of low resistance cells was significantly lower than that of wild type cells ( $P < 0.001$ ), the apoptosis rate of middle resistance cells was significantly lower than that of low resistance cells ( $P < 0.001$ ), and the apoptosis rate of high resistance cells was significantly lower than that of middle resistance cells ( $P < 0.05$ ). In the treatment group, the apoptosis rate of low resistance cells was significantly lower than that of wild type cells ( $P < 0.0001$ ), the apoptosis rate of middle resistance cells was significantly lower than that of low resistance cells ( $P < 0.0001$ ), the apoptosis rate of high resistance cells was significantly lower than that of middle resistance cells ( $P < 0.0001$ ).

### **Migratory and invasive capacities are elevated in T24-RC48**

ImageJ quantification showed that the number of migrating cells increased with resistance level: wild type ( $752 \pm 31.6$ ), low resistance ( $894 \pm 144.3$ ), middle resistance ( $978 \pm 133.9$ ), and high resistance ( $1252 \pm 338.3$ ). Significant differences were observed only between wild-type and high-resistant groups ( $P < 0.01$ ) ([Fig. 2e-f](#)).

Similarly, in invasion assays, high resistance cells showed significantly higher invasion capacity compared to wild type ( $P < 0.0001$ ), with no significant difference between wild type and low resistance groups (Fig. 2g-h).

### **Transcriptomic alterations highlight pathways associated with resistance**

Differential gene expression analysis showed the highest number of upregulated genes in the high resistance vs. wild type comparison. Reactome pathway analysis revealed enrichment in extracellular matrix organization<sup>9</sup> (involving genes like ICAM1 and DSP), GPCR ligand binding, and peptide ligand-binding receptors (Fig. 3a). DO (Disease Ontology) enrichment analysis showed significant association with urinary system disease (Fig. 3b). GO analysis indicated enrichment in angiogenesis<sup>10</sup> (BP, in which VEGF was a top hit), extracellular matrix (CC), and receptor regulator activity (MF) (Fig. 3c). KEGG pathways included cytokine-cytokine receptor interaction<sup>11</sup> (featuring IL1 $\beta$  and CD274/PD-L1) and cell adhesion molecules<sup>12</sup> (Fig. 3d). List of differentially expressed genes by transcriptome sequencing is provided in Document S1.

### **Proteomic analysis identifies key protein expression changes**

The highest number of differentially expressed proteins was found in the high resistance vs Wild type comparison. Domain enrichment analysis showed significant hits in armadillo-type fold and NAD(P)-binding domain (Fig. 3e). GO terms included immune response to tumor cell (BP, involving genes like PD-L1), superoxide dismutase activity (MF, involving genes like SOD2), and nucleus (CC) (Fig. 3f). KEGG pathways were enriched in metabolic pathways (including antioxidant enzymes such as SOD2 and CAT) (Fig. 3g). Proteins like RBPJ<sup>13</sup> and PD-L1<sup>14</sup> were also significantly upregulated in the resistant cells, corroborating the transcriptomic findings. Candidate list of key proteins in proteomic sequencing is provided in Document S1.

### **Integrated multi-omics analysis uncovers consensus resistance mechanisms**

A total of 120 common differentially expressed genes were identified through Venn analysis. Among these, 118 exhibited consistent expression trends, with 76 commonly upregulated and 42 commonly downregulated (Fig. 3h). This core gene set included several key players implicated in resistance, such as PD-L1, RBPJ, SOD2, CAT, DSP, ICAM1, and IL1 $\beta$ , which were selected for further validation. GO enrichment included immune-related processes (BP, e.g., PD-L1), cell adhesion molecule binding (MF, e.g., ICAM1), and cell-substrate junction (CC) (Fig. 3i, j). KEGG pathways included cytokine-cytokine receptor interaction<sup>15</sup> (e.g., IL1 $\beta$ ) and transcriptional misregulation<sup>16</sup> in cancer (Fig. 3k). List of key genes obtained from combined proteomic and transcriptomic analysis is provided in Document S1.

Notably, the expression of RBPJ and PD-L1 increased with higher resistance levels in both transcriptomic and proteomic analyses.

In addition, we applied advanced bioinformatic approaches to further elucidate the regulatory mechanism underlying drug resistance. Specifically, transcriptomic and proteomic profiles were analyzed across wild-type and low, medium, and high resistance groups. Genes showing significant alterations (ANOVA,  $P < 0.05$ ) at both transcriptional and protein levels were identified. Transcription factor enrichment analysis was performed using the TRRUST database, and key transcription factors were prioritized based on the concordance of their expression trends across increasing drug resistance levels at both transcript and protein levels. This systematic approach revealed that RBPJ, a Notch pathway protein, exhibited a stepwise increase in expression with escalating resistance—evident in both transcriptomic and proteomic analyses ([Fig. 3l](#)). Moreover, RBPJ was identified as a potential upstream regulator of angiogenesis-related processes enriched in transcriptomic GO analysis and immune response to tumor cell pathways highlighted in proteomic GO analysis, suggesting its role in modulating potential resistance-associated genes such as VEGF and PD-L1.

### **qRT-PCR validation confirms dysregulation of key resistance-related genes**

To validate the key resistance-related genes and pathways identified through our integrated transcriptomic and proteomic analyses, we performed quantitative real-time PCR (qRT-PCR) to examine their mRNA expression levels.

PD-L1 expression was significantly upregulated in all resistant groups compared to wild type T24 cells ( $P < 0.0001$ ) ([Fig. 4a](#)). VEGF expression was consistently increased in all resistant cells ( $P < 0.0001$ ) ([Fig. 4b](#)). RBPJ, a key transcriptional regulator of the Notch pathway<sup>13</sup>, showed no significant change in low resistance cells but was markedly increased in middle and high resistance groups ( $P < 0.0001$ ) ([Fig. 4c](#)). SOD2, encoding manganese superoxide dismutase, was significantly elevated across all resistant groups ( $P < 0.01$  to  $P < 0.0001$ ) ([Fig. 4d](#)). CAT (catalase) expression was significantly downregulated in all resistant groups ( $P < 0.0001$  to  $P < 0.001$ ) ([Fig. 4e](#)). DSP (desmoplakin) exhibited no change in low resistance cells but was significantly upregulated in middle and high resistance cells ( $P < 0.0001$ ) ([Fig. 4f](#)). ICAM1 was significantly increased in all resistant groups ( $P < 0.05$  to  $P < 0.0001$ ) ([Fig. 4g](#)). IL1 $\beta$  showed no change in low resistance cells but was significantly upregulated in middle and high resistance cells ( $P < 0.01$  to  $P < 0.0001$ ) ([Fig. 4h](#)).

### **Western Blot analysis confirms upregulation of RBPJ protein in RC48-resistant cells**

To further validate the protein expression of RBPJ, a key transcriptional regulator of the Notch signaling pathway, we performed Western blot analysis on T24 wild-type and T24-RC48 cells with varying resistance levels. Consistent with the transcriptomic and proteomic sequencing data, RBPJ protein expression was significantly elevated in the high resistance T24-RC48 cells compared to the wild-type T24 ( $P < 0.0001$ ). A significant increase was also observed in the middle resistance group ( $P < 0.05$ ), whereas the low resistance group showed no statistically significant difference relative to wild-type cells (Fig. 4i, j). These results corroborate the multi-omics findings and reinforce the role of RBPJ-mediated Notch signaling activation in the acquisition of RC48 resistance in bladder cancer.

### **Pro-angiogenic capacity is elevated in T24-RC48 and inhibited by Ivonescimab**

Under light microscopy at 2 hours, Human Umbilical Vein Endothelial Cells (HUVECs) began to migrate and connect, forming initial network structures in all groups, with no overt differences observed between conditions or cell lines (Fig. 5a-h). By 4 hours, the tubular networks became more pronounced and extensive. Conditioned media from middle and high resistance T24-RC48 cells appeared to promote more robust tube formation compared to that from parental T24 cells under drug-free conditions (Fig. 5i-p). At the 12-hour time point, the tube networks were mature and stable. The enhanced pro-angiogenic effect of conditioned media from high-resistance cells was visually more distinct compared to the parental control (Fig. 5q-x).

Statistical analysis of the number of junction points quantified these observations. At 2 hours, Ivonescimab significantly reduced junction points only in the high-resistance group compared to the untreated control ( $P < 0.05$ ), with no significant differences in parental, low, or middle resistance cells (Fig. 5y). At 4 hours, Ivonescimab again significantly decreased junction points in the high-resistance group ( $P < 0.05$ ), but not in other groups (Fig. 5y). Similarly, at 12 hours, high-resistance T24-RC48 showed a significant reduction in junction points upon Ivonescimab treatment ( $P < 0.05$ ), while other groups remained unaffected (Fig. 5y). In the absence of Ivonescimab, at 4 hours, conditioned media from middle-resistance T24-RC48 significantly increased junction points relative to parental T24 ( $P < 0.05$ ), as did high-resistance T24-RC48 ( $P < 0.05$ ) (Fig. 5z). At 12 hours, high-resistance T24-RC48 conditioned media further enhanced junction points compared to parental T24 ( $P < 0.01$ ) (Fig. 5z). No other comparisons reached statistical significance.

## Discussion

The development of resistance to antibody-drug conjugates like RC48 is a major clinical challenge. Our multi-omics investigation reveals that acquired resistance in bladder cancer is a multifaceted phenotype driven primarily by transcriptional and proteomic adaptations.

Our phenotypic data clearly demonstrate that T24-RC48 exhibit not only reduced drug sensitivity, but also enhanced migratory and invasive capabilities. These traits are consistent with a more aggressive cancer phenotype often linked to treatment resistance and disease progression<sup>17</sup>. Furthermore, flow cytometry revealed attenuated G2/M arrest and reduced apoptosis upon RC48 treatment in T24-RC48, indicating evasion of RC48's cytotoxic mechanism.

Multi-omics integration pinpointed several consistently dysregulated genes and pathways. Notably, we observed upregulation of VEGF and PD-L1. VEGF overexpression is a well-established mechanism promoting angiogenesis, and it has been implicated in resistance to various targeted therapies<sup>18</sup>. Similarly, PD-L1 upregulation may enable tumors to evade host immune surveillance<sup>19</sup>. These findings align with recent studies emphasizing the tumor microenvironment's role in modulating ADC efficacy<sup>20</sup>.

Additionally, activation of the Notch signaling pathway emerged as a likely contributor to resistance. Notch signaling is known to promote cancer stemness, epithelial-mesenchymal transition (EMT), and chemoresistance<sup>21</sup>. Our results suggest that Notch activation may help sustain cell survival and proliferative signals.

The significant downregulation of CAT (catalase) and upregulation of SOD2 (superoxide dismutase 2)<sup>22</sup> indicate altered redox homeostasis in T24-RC48, which may afford protection against RC48-induced cytotoxicity, as MMAE-mediated apoptosis often involves reactive oxygen species (ROS) generation<sup>23</sup>.

Our omics data also highlighted the involvement of cell adhesion and inflammation-related genes such as ICAM1<sup>24</sup> and IL1 $\beta$ , suggesting that inflammatory pathways and cell-matrix interactions may further support survival under drug stress.

Multi-omics and functional analyses consistently identified the upregulation of PD-L1 and VEGF in T24-RC48, which was associated with activation of the Notch signaling pathway. To illustrate the potential crosstalk between these pathways and their collective contribution to RC48 resistance, we propose a signaling network model where Notch activation transcriptionally promotes PD-L1 and VEGF expression, facilitating immune evasion and

angiogenesis, respectively (Fig. 6)<sup>25-28</sup>. This model provides a mechanistic basis for the phenotypic changes, which carries important clinical implications. The co-upregulation of PD-L1 and VEGF supports a combinatorial therapeutic approach using bispecific agents like Ivonescimab (anti-PD-1/VEGF)<sup>29</sup>. This strategy could potentially reverse resistance by normalizing vasculature and reactivating antitumor immunity. Previous studies have already demonstrated promising results with RC48 in combination with immune checkpoint inhibitors<sup>30</sup> or antiangiogenics<sup>31</sup>, and our data provide a mechanistic rationale for such synergies.

Notably, whole-genome sequencing revealed an average of 3,155,367 single nucleotide polymorphisms (SNPs) and 923,236 insertions/deletions (InDels) per sample. Detailed sequencing analysis data are provided in Document S1. However, no recurrent mutations directly associated with RC48-resistance were identified, suggesting that this category of genomic alterations may not be the primary driver of resistance in T24-RC48.

In conclusion, this study delineates a complex resistance landscape in RC48-treated BLCA, involving Notch signaling, oxidative stress, angiogenesis, and immune evasion. These results not only advance our understanding of RC48 resistance but also pave the way for biomarker-driven combination regimens to overcome resistance and improve patient outcomes.

## Methods

### Construction and preservation of drug-resistant cell lines

- **Cell culture**

Thaw the human bladder transitional cell carcinoma cell line T-24 and transfer the cell suspension into a T25 culture flask. Add complete McCoy's 5A medium (supplemented with 10% fetal bovine serum and 1% penicillin-streptomycin) till 5 ml. Label the flask with the cell line name (T-24) and experiment date on the side. Place the flask in a 37°C, 5% CO<sub>2</sub>, saturated humidity, normoxic incubator. Check cell attachment and viability next day.

- **Determination of drug IC<sub>50</sub> using CCK-8 assay**

Cells in the logarithmic growth phase were harvested to prepare a cell suspension, which was then seeded into a 96-well plate at a density of 4×10<sup>3</sup> cells per well. After overnight incubation to allow cell attachment, expose the cells to a series of diluted concentrations of RC48 (0, 1, 5, 10, 50, 100, 200, 300, 400, 500 µg/ml) and continue to culture for 72 hours. Remove the culture medium and add medium containing 10% CCK-8 reagent. Incubate the cells in a constant

temperature incubator for 1 hour, then measure the absorbance using an enzyme-linked immunosorbent assay (ELISA) reader. Analyze the experimental data to calculate the cell growth inhibition rate, plot the graph depicting the relationship between cell viability and drug concentration to obtain the half-inhibitory concentration ( $IC_{50}$ ), which determines the initial concentration of RC48.

- **Construction of T24-RC48 cell line**

T24 cells were initially cultured in complete medium. After seeding the cells into 6-well plates and T25 flasks, replaced the medium with fresh complete culture medium containing RC48 at the  $IC_{50}$  concentration (40  $\mu$ g/ml) at 24 hours post-seeding. Following 24 hours of RC48 treatment, renewed the drug-free medium and continued culturing until cells reached 80% confluence, then passaged them once. Cyclically repeated this procedure while incrementally elevating RC48 concentrations until the cells can survive and proliferate normally after 24-hour exposure to 100  $\mu$ g/ml RC48. Subsequently, we extended the treatment duration to 48 hours while maintaining the induction protocol. The concentration escalation sequence followed this order: 40  $\mu$ g/ml, 50  $\mu$ g/ml, 70  $\mu$ g/ml, 100  $\mu$ g/ml, 150  $\mu$ g/ml, 250  $\mu$ g/ml, 300  $\mu$ g/ml, 400  $\mu$ g/ml, and 500  $\mu$ g/ml. Through iterative adaptation cycles, the cells developed tolerance to progressively higher RC48 concentrations, ultimately yielding the RC48-resistant T24-RC48 cell line.

- **Assessment of drug resistance and stability in T24-RC48 cells**

Seed T24-RC48 and T24 control cells in 96-well plates ( $4 \times 10^3$  cells/well). After overnight adherence, add RC48 at varying concentrations (0, 1, 5, 10, 50, 100, 200, 300, 400, 500  $\mu$ g/ml). Remove the culture medium after 72 hours and calculate cell viability using the CCK-8 assay as described. Plot dose-response curves with RC48 concentration as the x-axis and cell survival rate as the y-axis. Determine the  $IC_{50}$  of the resistant cells and calculate the resistance index (RI) using the formula:  $RI = IC_{50} \text{ of T24-RC48} / IC_{50} \text{ of T24}$ .

For stability evaluation, discontinue RC48 treatment in T24-RC48 cells and maintain routine culture with normal medium replacement and passaging. After 3 weeks, repeat the above drug sensitivity assay. If the resistance index shows a minor decline but remains significantly elevated compared to parental cells, confirm stable drug resistance in T24-RC48 cells unaffected by passaging. Proceed with downstream experiments using this stabilized resistant

cell line.

- **Preservation of T24-RC48 drug-resistant cells**

After establishing the bladder cancer-resistant cell line, cryopreserve T24-RC48 cells in logarithmic growth phase using the following protocol: Replace the culture medium with antibiotic/antimycotic-free medium 24 hours before freezing. Prepare cryopreservation solution containing 90% fetal bovine serum and 10% DMSO. Aliquot 1.2 ml cell suspension into 1.8 ml cryovials. Label cryovials with cell line name and identification number on tube walls. Place cryovials in a programmable freezing container and store at -80°C overnight. Transfer cryovials to liquid nitrogen for long-term storage. Ship 10 cryovials on dry ice to the China Center for Type Culture Collection (CCTCC) at Wuhan University for official deposition.

### **Evaluation of drug-resistant cell lines**

- **Growth curve determination**

Seed low, middle, and high resistance cells along with T24 control cells in 6 numbered 96-well plates after trypsinization. Distribute each cell type across 12 wells ( $3 \times 10^3$  cells/well) and add 100  $\mu$ l complete medium. Incubate at 37°C with 5% CO<sub>2</sub> overnight. For plates 2-6, replace medium in 6 randomly selected wells per plate with fresh medium containing 200  $\mu$ g/ml RC48. Designate this timepoint as Day 0. Maintain all plates under standard culture conditions. For plate 1, add CCK-8 reagent according to manufacturer's instructions. Incubate for 1 hour and measure absorbance at 450 nm using a microplate reader. Repeat CCK-8 measurement on plates 2-6 every 24 hours using identical procedures. Plot cell proliferation curves with RC48 treatment duration as the x-axis and 450 nm absorbance values as the y-axis.

- **Cell migration assay**

Pre-culture cells in 1% serum medium for 24 hours. Add 600  $\mu$ l high-serum (20%) medium to the lower chamber. Position Transwell chambers into the medium without generating bubbles. Trypsinize cells, prepare suspensions in low-serum medium, and seed  $3 \times 10^4$  cells/200  $\mu$ l into each upper chamber. Incubate for 24 hours. Remove non-migrated cells from the upper chamber surface by gentle PBS wiping. Fix migrated cells with 4% paraformaldehyde for 15 minutes. Rinse twice with PBS. Stain cells with 0.1% crystal violet for 10 minutes. Rinse gently to remove excess dye. Mount stained chambers on moist glass slides. Capture images along

crosshair alignment lines for quantitative analysis.

- **Transwell invasion assay**

Dilute Matrigel with serum-free medium (1:8 ratio) at 4°C. Uniformly coat the upper surface of Transwell chambers with the diluted Matrigel. Incubate at 37°C for 3 hours to polymerize and aspirate excess liquid. Add low-serum medium cell suspension to the Matrigel-coated upper chambers. Fill lower chambers with 20% serum medium. Assemble chambers in 24-well plates and culture cells for 48 hours under standard conditions. Remove non-invasive cells from upper chambers by gentle PBS wiping. Fix invaded cells with 4% paraformaldehyde for 15 minutes. Rinse twice with PBS. Stain cells with 0.1% crystal violet for 10 minutes. Rinse to remove residual dye. Mount chambers on moist glass slides. Capture invasion images along crosshair markers using microscopy.

- **Flow cytometry assays**

- (1) **Cell Cycle Analysis**

Seed low-, middle-, high-resistance T24 cells and wild-type T24 cells in duplicate 6-well plates (2 wells per cell type). Treat one well of each cell type with RC48 at 24 hours post-seeding. Collect cells after 36 hours. Aspirate medium and trypsinize adherent cells. Centrifuge cell suspensions at 1000 rpm for 5 minutes and discard supernatant. Stain cells with propidium iodide (PI) for 30 minutes before flow cytometry. Analyze cell cycle distribution using a flow cytometer. Process raw data with FlowJo software.

- (2) **Apoptosis Detection**

Seed low-, middle-, high-resistance T24 cells and wild-type T24 cells in duplicate 6-well plates (2 wells per cell type). Treat one well of each cell type with RC48 at 24 hours post-seeding. Maintain the second well as untreated control. Collect all cells 48 hours post-treatment. Aspirate medium and process cells according to the apoptosis detection kit instructions. Analyze apoptotic rates using a flow cytometer. Quantify results with FlowJo software.

## **Multi-omics to explore the mechanism of cell resistance**

- **Transcriptome sequencing**

Culture low-, middle-, high-resistance T24 cells and wild-type T24 cells in 10 cm dishes until reaching 80% confluence. Rinse cells once with 4°C PBS. Add 1 ml TRIzol reagent per  $1 \times 10^7$

cells. Thoroughly pipette the reagent across the culture surface using a 1 ml pipette tip to ensure complete cell lysis. Transfer lysate to RNase-free 2 ml centrifuge tubes. Mechanically disrupt cell clusters by repeatedly drawing/ejecting the lysate through a sterile syringe until achieving a clear, non-viscous solution. Flash-freeze samples in liquid nitrogen. Store at -80°C prior to sequencing. Ship samples to the sequencing facility on dry ice. Total RNA sequencing was performed on the Illumina NovaSeq 6000 platform (PE150). After quality control and adapter trimming, reads were aligned to the GRCh38 reference genome using STAR, and gene expression levels were quantified.

- **Proteome sequencing**

Culture low-, middle-, high-resistance T24 cells and wild-type T24 cells in 10 cm dishes until reaching 80% confluence. Aspirate culture medium and add 4°C pre-chilled PBS to cover the cell monolayer. Gently rock the dish for 1 minute then aspirate PBS. Repeat PBS washing twice to completely remove residual medium. Place the dish on ice and add fresh 4°C pre-chilled PBS. Scrape cells to one side of the dish using a sterile cell scraper. Tilt the dish on ice to concentrate PBS-cell suspension. Transfer the cell suspension to pre-chilled centrifuge tubes using a pipette. Centrifuge and aspirate supernatant. Flash-freeze cell pellets in liquid nitrogen and store them at -80°C prior to sequencing. Ship samples to the sequencing facility on dry ice. Proteomic analysis was conducted using liquid chromatography-tandem mass spectrometry (LC-MS/MS) on a Q Exactive HF-X mass spectrometer. Proteins were identified and quantified using MaxQuant software against the UniProt human database.

- **Transcription analysis validation (qRT - PCR)**

Extract total RNA from cells ( $\geq 80\%$  confluence) using TRIzol reagent. Reverse transcribe RNA into cDNA using reverse transcriptase. Prepare reactions with predesigned gene-specific primers. Perform amplification and detection using a real-time PCR system. Record threshold cycle (Ct) values for target and housekeeping genes. Normalize data using housekeeping genes or standard curve methods. Calculate relative gene expression levels via  $\Delta\Delta Ct$  method. Primer sequence used in qRT - PCR are provided in Document S1.

- **Protein expression analysis validation (Western blotting)**

Extract and quantify protein samples from experimental and control groups. Separate proteins via SDS-PAGE gel electrophoresis. Transfer proteins to a solid-phase membrane using

electroblotting. Block the membrane with 5% non-fat milk/TBST to prevent nonspecific binding. Incubate with primary antibodies specific to target proteins (4°C overnight). Remove unbound antibodies by washing 3× with TBST. Apply HRP-conjugated secondary antibodies for 1 hour at room temperature. Wash membranes 3× with TBST. Visualize target protein bands using chemiluminescence detection reagents. Capture images with a chemiluminescence imaging system. Perform qualitative/semi-quantitative analysis using Image Lab™ software.

## **Function verification**

- Vascular formation**

Conditioned media were collected from T24 wild-type cells and low, medium, and high resistance T24-RC48 cell lines, both untreated and treated with 300 µg/ml of the drug RC48 for 24 hours in serum-free medium. HUVECs were serum-starved for 12 hours prior to the assay. Matrigel matrix was thawed at 4°C, mixed with DMEM at a 2:1 ratio, and plated into 24-well plates (300 µl/well), followed by polymerization at 37°C for 30 minutes. HUVECs were trypsinized, resuspended in the conditioned media at a density of  $3 \times 10^5$  cells/ml, and seeded onto the Matrigel-coated wells (0.5 ml/well) with three replicates per condition. The plates were incubated at 37°C with 5% CO<sub>2</sub>. Tube formation was observed under a light microscope after 2h, 4h and 12h.

## **Statistical analysis**

- Cell-based experiments**

Data from flow cytometry, migration, and invasion assays were analyzed by one-way ANOVA for comparisons across multiple groups, followed by Student's t-test for direct comparisons between two groups. All experiments were performed with at least three independent replicates. Results are presented as mean ± SEM (Standard Error of the Mean).

- Multi-omics data analysis**

Transcriptome and proteomics sequencing data were analyzed using bioinformatics tools, including differential expression analysis, functional annotation, and pathway enrichment analysis. Differentially expressed genes and proteins were screened using the combined

screening method of Fold Change and P value.  $|\text{Log}_2(\text{FoldChange})| > 1$  and  $P \text{ value} < 0.05$  were set as the significance threshold. Pathway enrichment analysis was performed using Reactome/DO/GO/KEGG database to evaluate the significance of pathways related to drug resistance mechanism. Rank pathways by enrichment significance ( $P < 0.05$ ).

### ● Validation experiments

qRT-PCR and Western blot data were analyzed using Student's t-test to verify expression changes of candidate targets identified from multi-omics screening. All validation experiments included  $\geq 3$  biological replicates, with data expressed as mean  $\pm$  SEM. Analyses were performed using SPSS 21.0 and GraphPad Prism 8.0, with  $p < 0.05$  defined as statistically significant.

## Figures

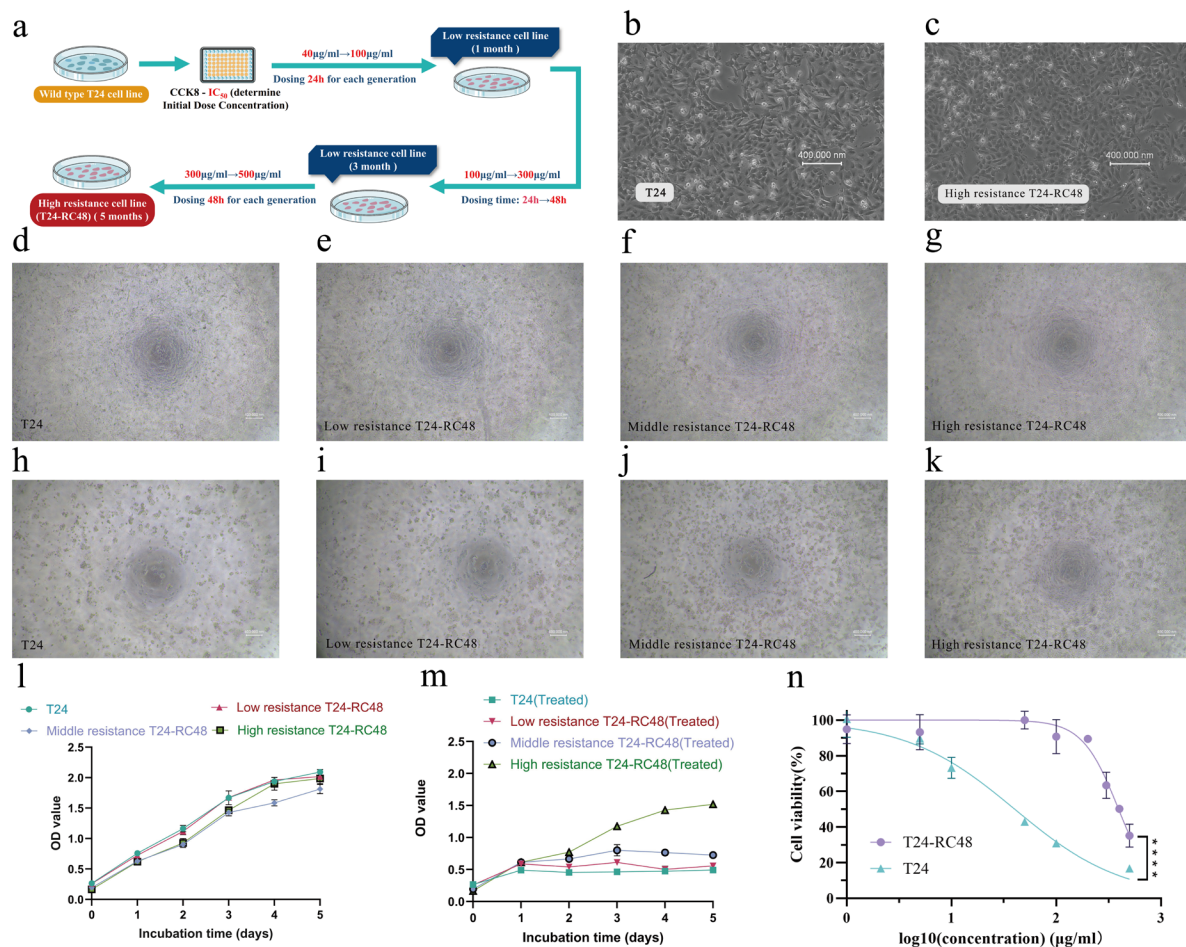


**Fig. 1 | Basic Phenotype Validation of T24 and T24-RC48.**

**a**, Schematic representation of directed evolution of resistance to RC48. **b-c**, Phase-contrast micrographs of parental T24 and low, middle, and high resistance T24-RC48 cells. **d-g**, Phase-contrast micrograph of parental T24 and low, middle, and high resistance T24-RC48 cells after 120 hours in drug-free medium. **h-k**, Phase-contrast micrograph of parental T24 and low, middle, and high resistance T24-RC48 cells after 120 hours of treatment with 200 μg/mL RC48. **l**, Dose-response curves of T24 and T24-RC48 cells treated with RC48 for 72 hours, as determined by the CCK-8 assay. Data are presented as mean ± SD (n=4). **m**, Growth curves of parental T24 and low, middle, and high resistance T24-RC48 cells under drug-free conditions over a period of 5 days, as assessed by the CCK-8 assay. Data are presented as mean ± SD (n=6). **n**, Growth curves of the indicated cell lines treated with a designated concentration of RC48 (200 μg/ml) over 5 days. Cell viability was measured daily. Data are presented as mean ± SD (n=6).

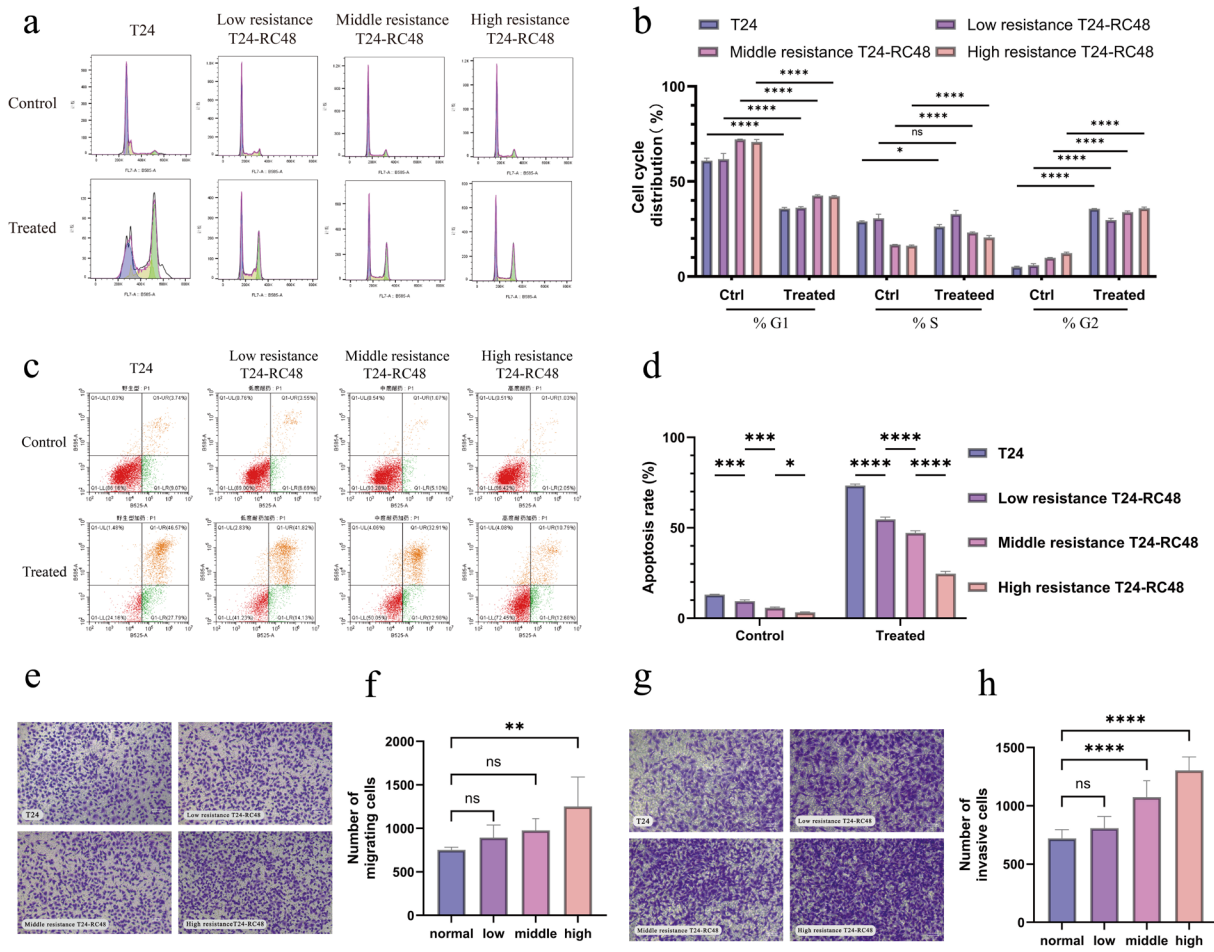


**Fig. 2 | Flow Cytometry Analysis and Transwell Assays of T24 and T24-RC48.**

**a**, Representative histograms of cell cycle distribution. **b**, Quantitative analysis of parental T24 and low, middle, and high resistance T24-RC48 cells' cell cycle distribution. Data are presented as mean  $\pm$  SD ( $n=3$ ). **c**, Representative flow cytometry dot plots of parental T24 and low, middle, and high resistance T24-RC48 cells' apoptosis. **d**, Quantitative analysis of apoptosis induction. Data are presented as mean  $\pm$  SD ( $n=3$ ). **e**, Representative images of migrated parental T24 and low, middle, and high resistance T24-RC48 cells in the Transwell migration assay. Data are presented as mean  $\pm$  SD ( $n=3$ ). **f**, Quantitative analysis of cell migration. **g**, Representative images of invaded parental T24 and low, middle, and high resistance T24-RC48 cells in the Transwell invasion assay. **h**, Quantitative analysis of cell invasion. Data are presented as mean  $\pm$  SD ( $n=3$ ). (ns, not significant, \*  $P < 0.05$ , \*\*  $P < 0.01$ , \*\*\*  $P < 0.001$ , \*\*\*\*  $P < 0.0001$ )

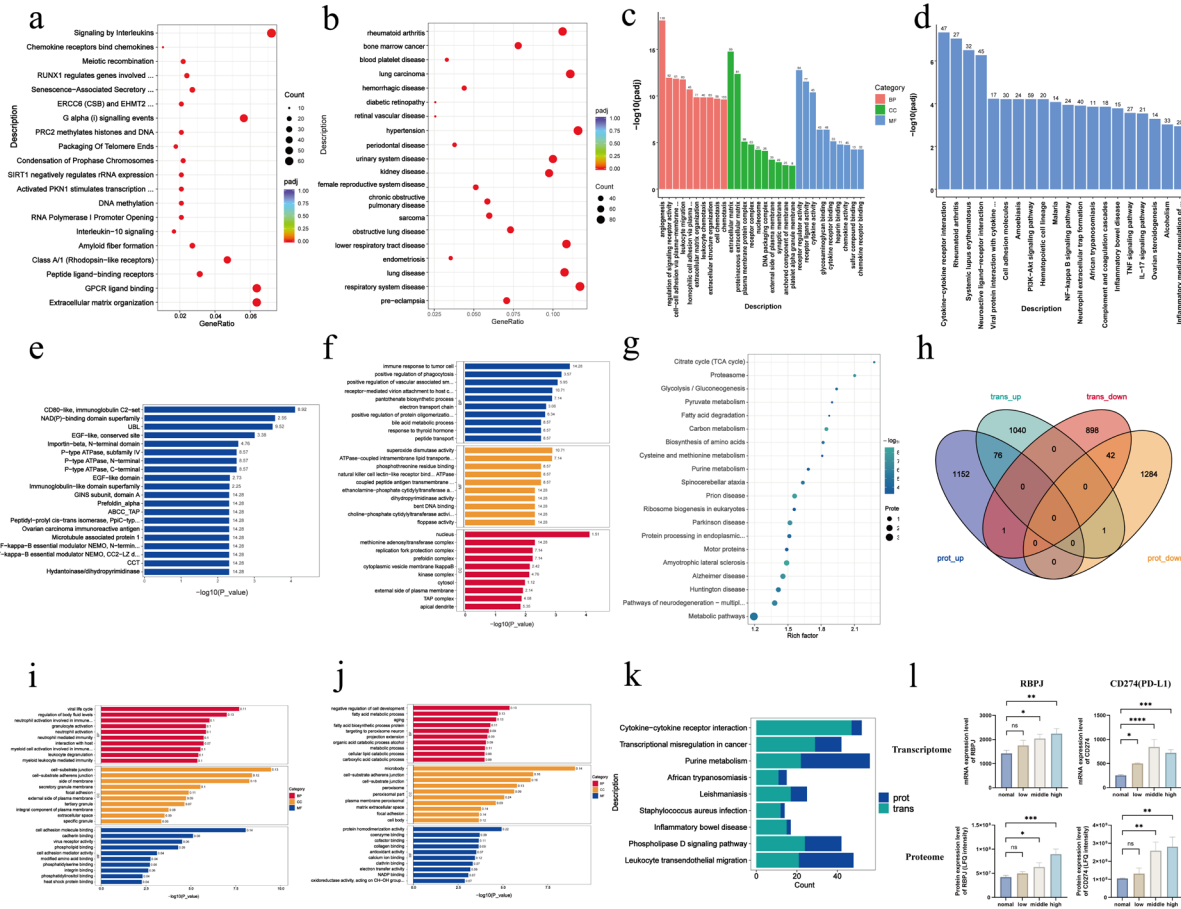


**Fig. 3 | Transcriptome and proteomic sequencing analysis of T24 and T24-RC48.**

**a**, Bubble plot of reactome pathway enrichment analysis of differentially expressed genes (DEGs) from transcriptomics. **b**, Bubble plot of DO (Disease Ontology) enrichment analysis of DEGs from transcriptomics. **c**, Bar chart of GO enrichment analysis of DEGs from transcriptomics. **d**, Bar chart of KEGG pathway enrichment analysis of DEGs from transcriptomics. **e**, Bar chart of Domain enrichment analysis of differentially expressed proteins (DEPs) from proteomics. **f**, Bar chart of GO enrichment analysis of DEPs from proteomics. **g**, Bubble plot of KEGG pathway enrichment analysis of DEPs from proteomics. **h**, Venn diagram illustrating the overlap between transcriptomic DEGs and proteomic DEPs. **i**, Bar chart of joint GO enrichment analysis of the co-upregulated genes/proteins identified in both transcriptomic and proteomic analyses (from 3H). **j**, Bar chart of joint GO enrichment analysis of the co-downregulated genes/proteins identified in both transcriptomic and proteomic analyses (from 3H). **k**, Bar chart of joint KEGG pathway enrichment analysis of the common genes/proteins identified in both omics analyses (from 3H). **l**, The expression trends of RBPJ and PD-L1 across different resistance levels, as measured by both transcriptomics (mRNA level) and proteomics (protein level). (ns, not significant, \*  $P < 0.05$ , \*\*  $P < 0.01$ , \*\*\*  $P < 0.001$ , \*\*\*\*  $P < 0.0001$ )

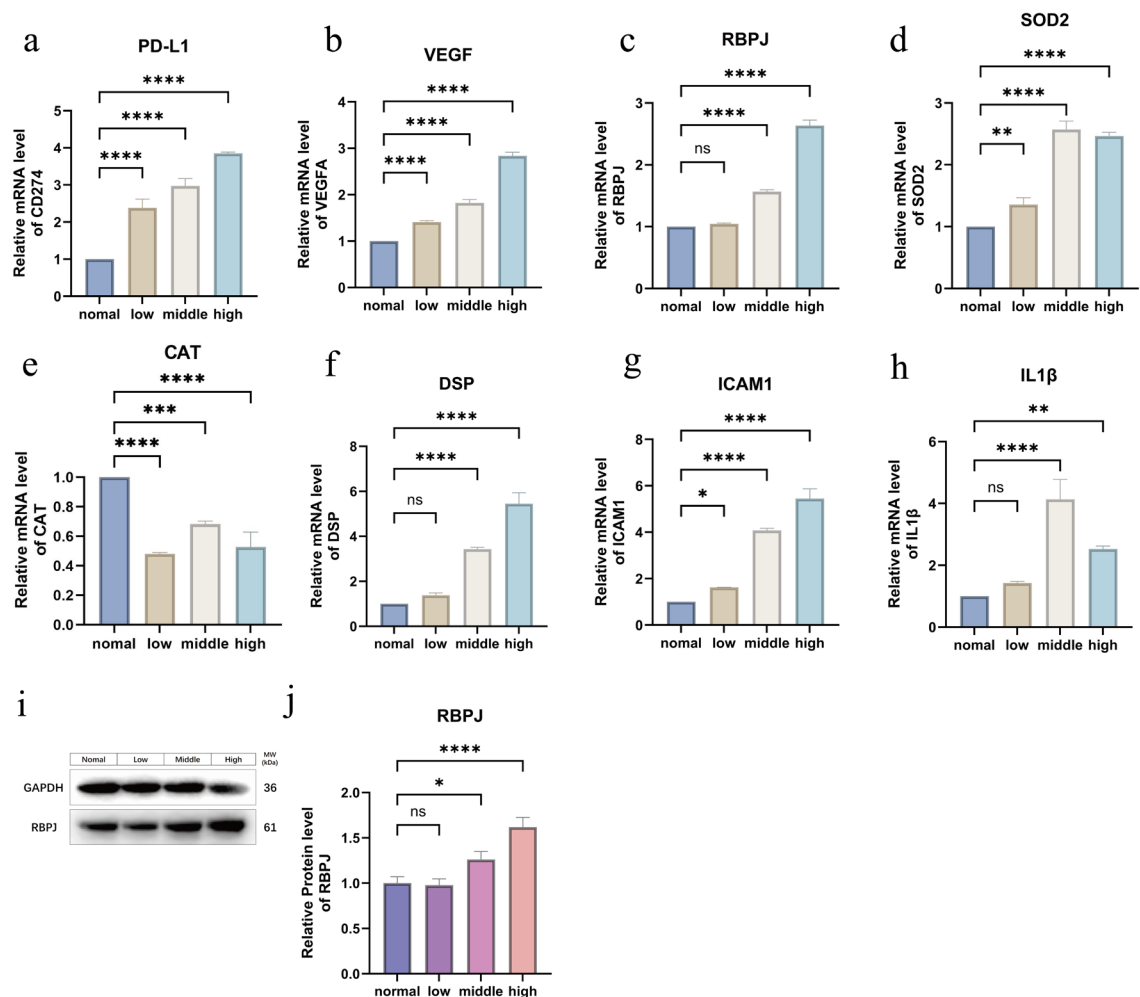


**Fig. 4 | Molecular Validation of T24 and T24-RC48.**

**a**, Expression level of PD-L1 in each group. Data are presented as mean  $\pm$  SD (n=3). **b**, Expression level of VEGF in each group. Data are presented as mean  $\pm$  SD (n=3). **c**, Expression level of RBPJ in each group. Data are presented as mean  $\pm$  SD (n=3). **d**, Expression level of SOD2 in each group. Data are presented as mean  $\pm$  SD (n=3). **e**, Expression level of CAT in each group. Data are presented as mean  $\pm$  SD (n=3). **f**, Expression level of DSP in each group. Data are presented as mean  $\pm$  SD (n=3). **g**, Expression level of ICAM1 in each group. Data are presented as mean  $\pm$  SD (n=3). **h**, Expression level of IL1 $\beta$  in each group. Data are presented as mean  $\pm$  SD (n=3). **i**, Representative Western blot images of RBPJ protein expression in parental T24 and low, middle, high resistance T24-RC48 cells. GAPDH was used as a loading control. **j**, Quantitative analysis of RBPJ protein expression levels normalized to GAPDH. Data are presented as mean  $\pm$  SD (n=3). (ns, not significant, \* P < 0.05, \*\* P < 0.01, \*\*\* P < 0.001, \*\*\*\* P < 0.0001)

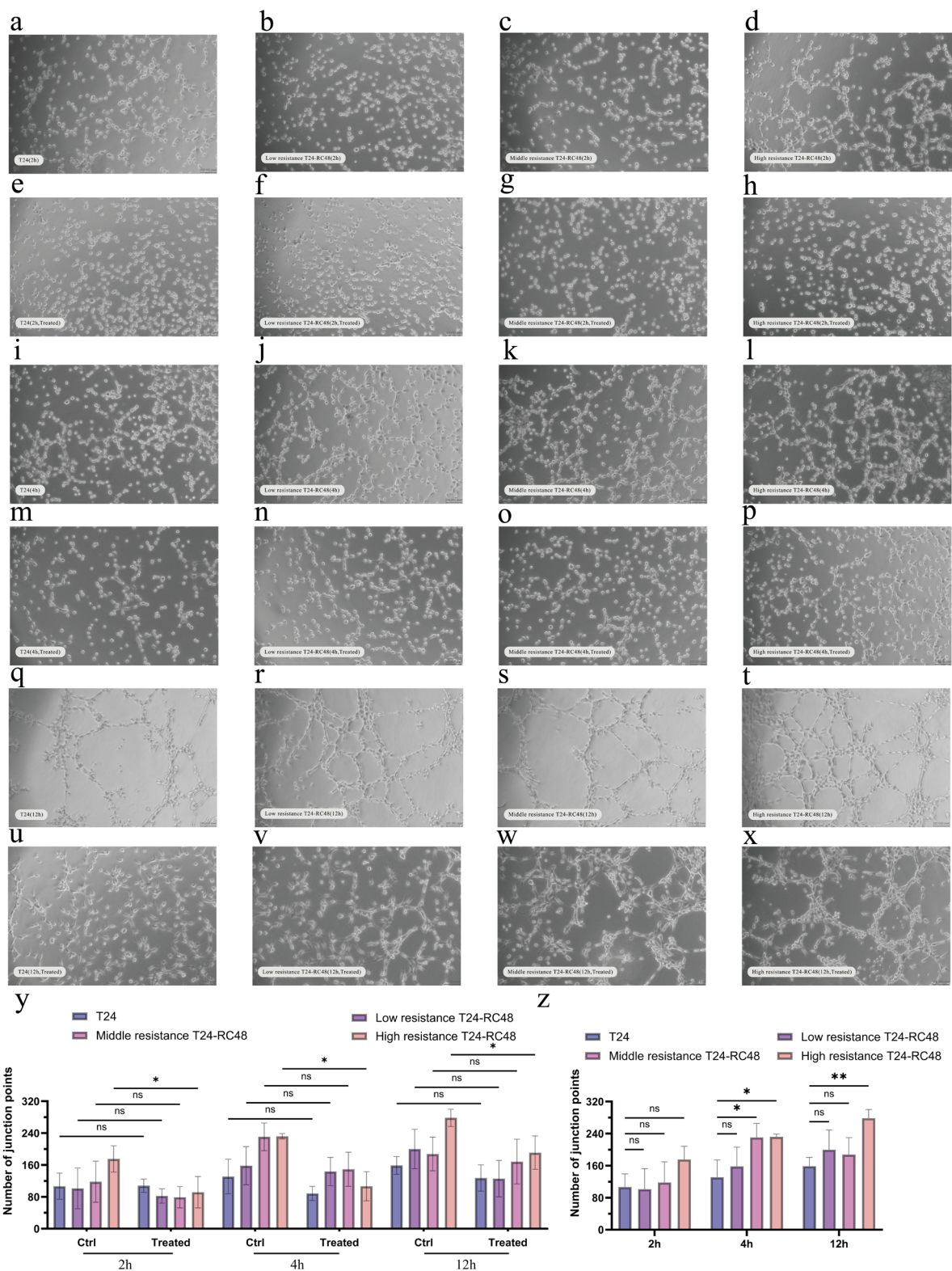


**Fig. 5 | Vascular formation of T24 and T24-RC48.**

**a-d**, Representative phase-contrast micrographs of HUVEC tube formation at 2 hours under drug-free conditions. HUVECs were co-cultured with conditioned media from: (a) parental T24, (b) low resistance T24-RC48, (c) middle resistance T24-RC48, and (d) high resistance T24-RC48. **e-h**, Representative images of HUVEC tube formation at 2 hours in the presence of Ivonescimab (300 µg/mL). HUVECs were co-cultured with conditioned media from: (e) parental T24, (f) low resistance T24-RC48, (g) middle resistance

T24-RC48, and (h) high resistance T24-RC48. **i-l**, Representative images of HUVEC tube formation at 4 hours under drug-free conditions. HUVECs were co-cultured with conditioned media from: (i) parental T24, (j) low resistance T24-RC48, (k) middle resistance T24-RC48, and (l) high resistance T24-RC48. **m-p**, Representative images of HUVEC tube formation at 4 hours in the presence of Ivonescimab (300 µg/mL). HUVECs were co-cultured with conditioned media from: (m) parental T24, (n) low resistance T24-RC48, (o) middle resistance T24-RC48, and (p) high resistance T24-RC48. **q-t**, Representative images of HUVEC tube formation at 12 hours point under drug-free conditions. HUVECs were co-cultured with conditioned media from: (q) parental T24, (r) low resistance T24-RC48, (s) middle resistance T24-RC48, and (t) high resistance T24-RC48. **u-x**, Representative images of HUVEC tube formation at 12 hours in the presence of Ivonescimab (300 µg/mL). HUVECs were co-cultured with conditioned media from: (u) parental T24, (v) low resistance T24-RC48, (w) middle resistance T24-RC48, and (x) high resistance T24-RC48. **y**, Quantitative analysis of the number of junction points in the HUVEC network following treatment with or without Ivonescimab. **z**, Quantitative analysis of the number of junction points in HUVECs cultured with conditioned media from different cell lines over time (2h, 4h, 12h) under drug-free conditions. Data are presented as mean ± SD (n=3). (ns, not significant, \* P<0.05, \*\* P<0.01)

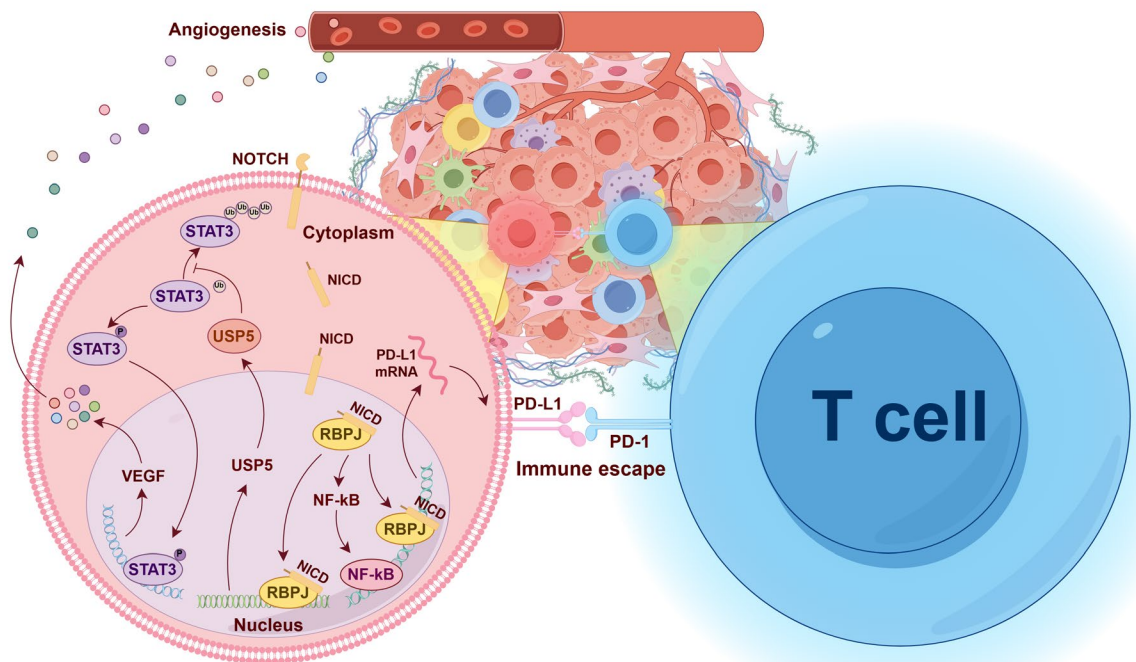


**Fig. 6 | Proposed signaling network linking Notch activation to PD-L1 and VEGF upregulation in RC48-resistant bladder cancer.**

Schematic representation of the hypothesized mechanism by which Notch pathway activation (via RBPJ-mediated transcription) leads to increased expression of PD-L1 and VEGF, contributing to immune escape and angiogenesis, respectively. These adaptations collectively promote RC48 resistance and tumor aggressiveness.

## **Supplemental information**

Document S1.

### **Acknowledgements**

Y.C.M. conceived the study and was the major contributor in writing the manuscript. Y.L.S., Y. B.F., B.S., and F.Y.C. contributed to data collection and analysis. S.X.Y., G.J.X., Y.X.Y., D.H.Y., S.X.R., G.S.Y., X.D., Z.C., and Z.Z.H. participated in results interpretation and discussion. L.J.H., G.M., K.Y., W.L.H., Z.S., and S.M.J. supervised the work, provided critical feedback, and revised the manuscript. All authors read and approved the final version.

The authors gratefully acknowledge the support from all colleagues and institutions involved in this research.

### **References**

1. Bray F, Laversanne M, Sung H, Ferlay J, Siegel RL, Soerjomataram I *et al.*, Global cancer statistics 2022: GLOBOCAN estimates of incidence and mortality worldwide for 36 cancers in 185 countries. *CA Cancer J Clin*, (2024).  
DOI: <https://doi.org/10.3322/caac.21834>
2. Wéber A, Vignat J, Shah R, Morgan E, Laversanne M, Nagy P *et al.*, Global burden of bladder cancer mortality in 2020 and 2040 according to GLOBOCAN estimates. *World journal of urology* **42**: 237, (2024).  
DOI: <https://doi.org/10.1007/s00345-024-04949-8>
3. Fu Z, Li S, Han S, Shi C, Zhang Y, Antibody drug conjugate: the "biological missile" for targeted cancer therapy. *Signal transduction and targeted therapy* **7**: 93, (2022).  
DOI: <https://doi.org/10.1038/s41392-022-00947-7>
4. Li M, Zhao X, Yu C, Wang L, Antibody-Drug Conjugate Overview: a State-of-the-art Manufacturing Process and Control Strategy. *Pharmaceutical research* **41**: 419-440, (2024).  
DOI: <https://doi.org/10.1007/s11095-023-03649-z>
5. He J, Zeng X, Wang C, Wang E, Li Y, Antibody-drug conjugates in cancer therapy: mechanisms and clinical studies. *MedComm* **5**: e671, (2024).  
DOI: <https://doi.org/10.1002/mco2.671>
6. Sheng X, Yan X, Wang L, Shi Y, Yao X, Luo H *et al.*, Open-label, Multicenter, Phase II Study of RC48-ADC, a HER2-Targeting Antibody-Drug Conjugate, in Patients with Locally Advanced or

- Metastatic Urothelial Carcinoma. *Clinical cancer research : an official journal of the American Association for Cancer Research* **27**: 43-51, (2021).  
DOI: <https://doi.org/10.1158/1078-0432.ccr-20-2488>
7. Wang D, Cao M, Zhang Y, Bi L, Chen M, Ni M *et al.*, RC48-ADC monotherapy or in combination with immunotherapy for locally advanced or metastatic urothelial carcinoma with HER2 low and null expression: a multicenter, real-world, retrospective study. *BMC cancer* **25**: 812, (2025).  
DOI: <https://doi.org/10.1186/s12885-025-14154-4>
8. Diaz-Rodriguez E, Gandullo-Sanchez L, Ocana A, Pandiella A, Novel ADCs and Strategies to Overcome Resistance to Anti-HER2 ADCs. *Cancers (Basel)* **14**, (2021).  
DOI: <https://doi.org/10.3390/cancers14010154>
9. Deb B, Patel K, Sathe G, Kumar P, N-Glycoproteomic Profiling Reveals Alteration In Extracellular Matrix Organization In Non-Type Bladder Carcinoma. *Journal of clinical medicine* **8**, (2019).  
DOI: <https://doi.org/10.3390/jcm8091303>
10. Huang X, Wang Q, Nan Y, Zhang X, Xu K, Ju D *et al.*, Targeting CD47 and Angiogenesis Demonstrates Effective Anti-Tumor Effect in Bladder Cancer. *Biomedicines* **12**, (2024).  
DOI: <https://doi.org/10.3390/biomedicines12092152>
11. He K, Meng X, Su J, Jiang S, Chu M, Huang B, Oleanolic acid inhibits the tumor progression by regulating Lactobacillus through the cytokine-cytokine receptor interaction pathway in 4T1-induced mice breast cancer model. *Heliyon* **10**: e27028, (2024).  
DOI: <https://doi.org/10.1016/j.heliyon.2024.e27028>
12. Griffiths TR, Brotherick I, Bishop RI, White MD, McKenna DM, Horne CH *et al.*, Cell adhesion molecules in bladder cancer: soluble serum E-cadherin correlates with predictors of recurrence. *British journal of cancer* **74**: 579-584, (1996).  
DOI: <https://doi.org/10.1038/bjc.1996.404>
13. Giaimo BD, Gagliani EK, Kovall RA, Borggrefe T, Transcription Factor RBPJ as a Molecular Switch in Regulating the Notch Response. *Advances in experimental medicine and biology* **1287**: 9-30, (2021).  
DOI: [https://doi.org/10.1007/978-3-030-55031-8\\_2](https://doi.org/10.1007/978-3-030-55031-8_2)
14. Jing W, Wang G, Cui Z, Xiong G, Jiang X, Li Y *et al.*, FGFR3 Destabilizes PD-L1 via NEDD4 to Control T-cell-Mediated Bladder Cancer Immune Surveillance. *Cancer research* **82**: 114-129, (2022).  
DOI: <https://doi.org/10.1158/0008-5472.can-21-2362>
15. Tan Z, Chen X, Huang Y, Fu S, Li H, Gong C *et al.*, Integrative multi-omics and machine learning identify a robust signature for discriminating prognosis and therapeutic targets in bladder cancer. *Journal of Cancer* **16**: 1479-1503, (2025).  
DOI: <https://doi.org/10.7150/jca.105066>

16. Isali I, McClellan P, Calaway A, Prunty M, Abbosh P, Mishra K *et al.*, Gene network profiling in muscle-invasive bladder cancer: A systematic review and meta-analysis. *Urologic oncology* **40**: 197.e111-197.e123, (2022).  
DOI: <https://doi.org/10.1016/j.urolonc.2021.11.003>
17. Chen O, Vovk O, Polishchuk N, Mayevska O, Shuvayeva G, Demir M *et al.*, Adaptation to Arginine Deprivation Leads to a More Aggressive, Therapy-Resistant Phenotype in HNSCC Cells. *Biomolecules* **15**, (2025).  
DOI: <https://doi.org/10.3390/biom15060900>
18. Hong S, Yu N, Cho JY, Lee GK, Ahn BC, Lee Y *et al.*, VEGF Signal Complexity Confers Resistance to Atezolizumab, Bevacizumab, Carboplatin, and Paclitaxel in EGFR-Tyrosine Kinase Inhibitor-Resistant Non-Small Cell Lung Cancer. *MedComm* **6**: e70335, (2025).  
DOI: <https://doi.org/10.1002/mco.2.70335>
19. Wangpaichitr M, Kandemir H, Li YY, Wu C, Nguyen D, Feun LG *et al.*, Relationship of Metabolic Alterations and PD-L1 Expression in Cisplatin Resistant Lung Cancer. *Cell & developmental biology* **6**, (2017).  
DOI: <https://doi.org/10.4172/2168-9296.1000183>
20. Dumontet C, Reichert JM, Senter PD, Lambert JM, Beck A, Antibody-drug conjugates come of age in oncology. *Nature reviews Drug discovery* **22**: 641-661, (2023).  
DOI: <https://doi.org/10.1038/s41573-023-00709-2>
21. Shi Q, Xue C, Zeng Y, Yuan X, Chu Q, Jiang S *et al.*, Notch signaling pathway in cancer: from mechanistic insights to targeted therapies. *Signal transduction and targeted therapy* **9**: 128, (2024).  
DOI: <https://doi.org/10.1038/s41392-024-01828-x>
22. Nikic P, Dragicevic D, Jerotic D, Savic S, Djukic T, Stankovic B *et al.*, Polymorphisms of Antioxidant Enzymes SOD2 (rs4880) and GPX1 (rs1050450) Are Associated with Bladder Cancer Risk or Its Aggressiveness. *Medicina (Kaunas, Lithuania)* **59**, (2023).  
DOI: <https://doi.org/10.3390/medicina59010131>
23. Zheng M, Wang Z, Li M, Yang N, Lu H, Zhang Z *et al.*, A novel SLC3A2-targeting antibody-drug conjugate exerts potent antitumor efficacy in head and neck squamous cell cancer. *Translational oncology* **45**: 101981, (2024).  
DOI: <https://doi.org/10.1016/j.tranon.2024.101981>
24. Liang T, Tao T, Wu K, Liu L, Xu W, Zhou D *et al.*, Cancer-Associated Fibroblast-Induced Remodeling of Tumor Microenvironment in Recurrent Bladder Cancer. *Advanced science (Weinheim, Baden-Wurttemberg, Germany)* **10**: e2303230, (2023).  
DOI: <https://doi.org/10.1002/advs.202303230>
25. Wang C, Yang M, Zhong Y, Cao K, Wang X, Zhang C *et al.*, Immunosuppressive JAG2+ tumor-associated neutrophils hamper PD-1 blockade response in ovarian cancer by mediating the

- differentiation of effector regulatory T cells. *Cancer Communications* **45**: 747-773, (2025).  
DOI: <https://doi.org/10.1002/cac2.70021>
26. Jin X, Ding D, Yan Y, Li H, Wang B, Ma L *et al.*, Phosphorylated RB Promotes Cancer Immunity by Inhibiting NF-κB Activation and PD-L1 Expression. *Molecular cell* **73**: 22-35.e26, (2019).  
DOI: <https://doi.org/10.1016/j.molcel.2018.10.034>
27. Li C, Wu P, Xie X, Chen X, Chen L, Zhu L *et al.*, Aberrant Notch-signaling promotes tumor angiogenesis in esophageal squamous-cell carcinoma. *Signal transduction and targeted therapy* **10**, (2025).  
DOI: <https://doi.org/10.1038/s41392-025-02309-5>
28. Chen L, Lu H, Peng D, Cao LL, Ballout F, Srirmajayam K *et al.*, Activation of NOTCH signaling via DLL1 is mediated by APE1-redox-dependent NF-κB activation in oesophageal adenocarcinoma. *Gut* **72**: 421-432, (2023).  
DOI: <https://doi.org/10.1136/gutjnl-2022-327076>
29. Frentzas S, Austria Mislang AR, Lemech C, Nagrial A, Underhill C, Wang W *et al.*, Phase 1a dose escalation study of ivonescimab (AK112/SMT112), an anti-PD-1/VEGF-A bispecific antibody, in patients with advanced solid tumors. *Journal for immunotherapy of cancer* **12**, (2024).  
DOI: <https://doi.org/10.1136/jitc-2023-008037>
30. Ge H, Liu C, Shen C, Hu D, Zhao X, Wang Y *et al.*, The effectiveness and safety of RC48 alone or in combination with PD-1 inhibitors for locally advanced or metastatic urothelial carcinoma: a multicenter, real-world study. *Journal of translational medicine* **23**: 243, (2025).  
DOI: <https://doi.org/10.1186/s12967-025-06237-4>
31. Li W, Zhang K, Wang W, Liu Y, Huang J, Zheng M *et al.*, Combined inhibition of HER2 and VEGFR synergistically improves therapeutic efficacy via PI3K-AKT pathway in advanced ovarian cancer. *Journal of experimental & clinical cancer research : CR* **43**: 56, (2024).  
DOI: <https://doi.org/10.1186/s13046-024-02981-5>